Research Square

Preprints are preliminary reports that have not undergone peer review.
They should not be considered conclusive, used to inform clinical practice,
or referenced by the media as validated information.

Segment-Level Gait Dynamics Reveal Early Parkinsonian Motor Signatures in Fall-Prone Older Adults

Bohyun Kim
Dong-A University
Changhong Youm
chyoum@dau.ac.kr

Dong-A University
Sang-Myung Cheon
Dong-A University
Hwayoung Park
Dong-A University
Juseon Hwang
Dong-A University
Minsoo Kim
Dong-A University

Research Article

Keywords: Parkinson's disease, Gait analysis, Wearable sensors, Deep learning, Digital biomarkers, Falls

Posted Date: June 19th, 2026

DOI: https://doi.org/10.21203/rs.3.rs-9786931/v1

License: This work is licensed under a Creative Commons Attribution 4.0 International License.
Read Full License

Additional Declarations: No competing interests reported.

Abstract

Background

Early detection of Parkinson's disease (PD) is limited by the late emergence of overt motor symptoms, while subtle gait abnormalities may appear years earlier. Older adults with recurrent unexplained falls have been suggested as a population with elevated prodromal PD risk, yet objective tools to quantify PD-like motor dynamics in this group remain scarce. We aimed to develop and validate a multi-channel time–frequency deep learning framework for segment-level identification of PD-like gait dynamics. Furthermore, we aimed to derive subject-level, model-defined transition metrics that characterize sustained PD-like motor states in fall-prone older adults.

Methods

Overall, 211 older adults (PD, n = 50; fall-prone older adults, n = 161) who completed inertial sensor–based gait assessment under slower (80%), preferred, and faster (120%) walking speeds were included. Data from 16 bilateral inertial measurement unit channels were transformed into continuous wavelet transform scalograms and used to train single- and multi-channel convolutional neural network models using subject-wise stratified five-fold cross-validation. Subject-level "transition" was defined as entry into a sustained PD-like state using smoothing and a hysteresis rule, with an operating threshold selected to control false positives (target false-positive rate [FPR] 5%).

Results

The multi-channel model achieved consistently high segment-level discrimination across speeds (area under the receiver operating characteristic curve [AUC]: faster 0.992 ± 0.007; preferred 0.974 ± 0.016; slower 0.975 ± 0.017), outperforming representative single-channel models (AUC: 0.65–0.75). Subject-level transition detection under the 5% FPR operating point yielded high sensitivity (0.96–1.00) with strong specificity (0.857–0.913) across speeds, while relaxing the FPR constraint to 10% substantially reduced specificity.

Conclusions

Multi-channel time–frequency deep learning enables robust identification of sustained PD-like gait states from short walking segments and provides interpretable model-derived transition metrics for motor risk stratification in fall-prone older adults.

Background

Parkinson's disease (PD) is a progressive neurodegenerative disorder characterized by impairments in motor control, postural stability, and gait regulation, and represents the second most common neurodegenerative condition worldwide [1]. Clinical diagnosis is typically established only after overt motor symptoms emerge, by which time approximately 50–60% of dopaminergic neurons have already degenerated [2, 3]. Increasing evidence suggests that subtle motor alterations may occur years before formal diagnostic criteria are met [2, 3]. Identifying these early motor changes has therefore become a central objective in PD research, because earlier detection may improve risk stratification and enable timely intervention strategies aimed at delaying functional decline [2, 3]. Despite this growing interest, objective approaches to detecting early motor vulnerability prior to clinical diagnosis remain limited [2, 4].

To facilitate earlier identification of individuals at risk for PD, the International Parkinson and Movement Disorder Society proposed research criteria that integrate multiple prodromal risk markers—including non-motor symptoms, autonomic dysfunction, sleep disturbances, and genetic susceptibility—to estimate future PD probability [3, 5]. These criteria have substantially advanced probabilistic risk stratification for prodromal PD [4, 6]. However, the current framework relies predominantly on clinical and non-motor indicators and only partially reflects objective motor dysfunction directly associated with functional mobility. Consequently, quantitative motor biomarkers that can capture early alterations in gait stability, postural regulation, and movement variability remain insufficiently incorporated into existing predictive models.

Recent epidemiological and clinical studies suggest that older adults experiencing recurrent unexplained falls may represent a population at higher risk for prodromal PD [7, 8]. Falls are highly prevalent in aging populations and are frequently associated with gait instability and cognitive–motor interference, including executive dysfunction—features that partially overlap with early parkinsonian motor characteristics [9–12]. Emerging evidence further indicates that fall-prone older adults may exhibit subtle mobility impairments that precede PD diagnosis, suggesting that fall vulnerability may reflect early neurodegenerative processes affecting motor control networks [7, 8, 13, 14]. Nevertheless, objective frameworks that can systematically quantify PD-like motor dynamics and characterize transition-related risk in this population remain limited [15].

Gait analysis provides a particularly promising avenue for addressing this challenge because locomotion requires continuous integration of motor planning, sensory feedback, and postural regulation across distributed neural systems [9, 16]. Parkinsonian gait is commonly characterized by increased variability, reduced movement automaticity, heightened attentional demand, impaired inter-limb coordination or asymmetry, and disrupted rhythmic regulation—features reflecting dysfunction within corticobasal ganglia–brainstem motor circuits [9, 10, 16]. Recent advances in wearable inertial sensing technologies have enabled quantitative characterization of gait dynamics beyond traditional clinical observation, supporting the emergence of digital motor biomarkers for neurological disorders [4, 17]. However, most existing analytical approaches rely on summary gait parameters averaged across walking trials, which

may obscure transient or context-dependent motor abnormalities occurring over short temporal intervals [4, 9].

In parallel, gait-based machine learning approaches for PD identification have gained increasing attention [18, 19]. Most prior studies have focused on subject-level classification using aggregated features derived from cross-sectional recordings [18, 19]. Such approaches implicitly assume motor impairment to be stable over time. However, PD-related motor deterioration is increasingly recognized as a gradual and dynamic process in which gait and balance impairments may fluctuate and appear intermittently, particularly under increased task demands [2, 9, 10]. As a result, averaging procedures may dilute early micro-level instability signals that precede overt behavioral differences at the individual level [4, 9]. Therefore, analytical frameworks that can capture short-duration motor fluctuations may be necessary to detect emerging PD-like motor dynamics before stable clinical manifestations become apparent. Such approaches may also support earlier identification of mobility-related vulnerability and facilitate timely implementation of targeted intervention strategies in clinically high-risk older adults.

Recent developments in deep learning provide new opportunities to model complex time-series signals without reliance on predefined feature engineering [19]. Time–frequency representations generated using continuous wavelet transforms (CWT) enable simultaneous characterization of temporal and spectral structures within inertial sensor signals [20]. When combined with multi-channel architectures integrating bilateral kinematic information, such models may capture coordinated motor signatures reflecting system-level motor control rather than isolated signal deviations [16, 19]. Importantly, this framework allows motor behavior to be examined as a dynamically evolving process, enabling identification of transient motor states that may reflect early instability within locomotor control systems.

Despite these advances, a critical gap remains; current analytical approaches rarely capture the temporal evolution of PD-like motor dynamics at fine temporal scales. Frameworks that can identify transient motor-state fluctuations—conceptualized as early markers of dynamic motor vulnerability—are largely absent from existing predictive models. Such approaches may be especially relevant in populations exhibiting intermittent mobility instability, such as older adults with recurrent falls, where early neurodegenerative motor signatures may emerge only under specific locomotor demands.

Therefore, this study aimed to develop and validate a multi-channel time–frequency deep learning framework for identifying sustained PD-like motor states using segment-level gait representations derived from wearable inertial sensors. Rather than relying solely on aggregated gait features, our approach models short-duration locomotor segments to capture dynamically evolving motor patterns. We further examined whether temporal metrics derived from prediction trajectories could characterize transition-related motor instability in older adults with a history of falls. Finally, we investigated whether increased locomotor demand during faster walking speed (FWS) would enhance the discriminability of PD-related motor patterns.

We hypothesized that:

1. Multi-channel integration of bilateral gait signals would improve discrimination of PD-like motor dynamics compared with single-channel models.
2. Segment-level temporal analysis would reveal transition patterns indicative of latent motor vulnerability within a fall-prone aging population.
3. FWS would enhance the discriminability of PD-related motor signatures due to increased locomotor control demands.

Methods

Participants

A total of 211 older adults participated in this study, including 50 with PD and 161 fall-prone individuals. The inclusion criteria for participants with PD were as follows: (a) a clinician-confirmed diagnosis of idiopathic PD according to the UK Parkinson's Disease Society Brain Bank Clinical Diagnostic Criteria, (b) age ≥ 50 years, and (c) a modified Hoehn and Yahr (H&Y) scale score of 1–3, indicating independent ambulation without the use of an assistive device. Participants were screened to ensure the absence of clinically significant cognitive impairment prior to enrollment. The fall-prone older adults were community-dwelling older adults aged 65 years or older with no diagnosis of PD or other neurological disorders and a self-reported history of at least one fall during the previous 12 months. Individuals with musculoskeletal, cardiovascular, vestibular, or neurological conditions that could have affected gait substantially within the previous 6 months were excluded.

Demographic and clinical characteristics of all participants are summarized in Table 1. This study was approved by the Institutional Review Board of Dong-A University Hospital (IRB number: DAUHIRB-22–089). All participants received a detailed explanation of the study procedures and provided written informed consent prior to participation. The study was registered in the Clinical Research Information Service of the Republic of Korea (KCT0009353).

Table 1
Demographic and clinical characteristics of study participants.

Characteristics	PDs (n = 50)	Fall-prone older adults (n = 161)
Sex (male/female)	26/24	37/124
Age (years)	68.4 ± 7.0	74.6 ± 5.0
Height (cm)	161.7 ± 8.5	155.8 ± 8.1
Body mass (kg)	63.5 ± 10.6	59.6 ± 9.2
BMI (kg/m^2)	24.2 ± 2.6	24.5 ± 3.3
H&Y scale (stages)	2.0 ± 0.7	
UPDRS total (scores)	55.7 ± 19.9	
UPDRS part III (scores)	32.5 ± 13.9	
L-DOPA equivalent dose (mg/day)	560.8 ± 331.2	
Treatment duration (years)	5.0 ± 3.6	
Symptom duration (years)	5.8 ± 3.7	

Data are presented as mean ± standard deviation unless otherwise indicated. PD, Parkinson's disease; BMI, body mass index; H&Y, Hoehn and Yahr; UPDRS, Unified Parkinson's Disease Rating Scale; L-Dopa equivalent dose, daily levodopa equivalent dosage.

Test procedures and data analysis

Gait analysis was conducted using shoe-type data loggers (Smart Balance® SB-1, JEIOS, Korea) equipped with inertial measurement units (IMUs) embedded in the shoe outsole. Each IMU recorded tri-axial acceleration (± 6 g) and angular velocity (± 500°/s) along three orthogonal axes, with data transmitted wirelessly to a gait analysis system (DynaStab™, JEIOS, Korea).

Participants with PD performed the gait assessment while in the "ON" state of antiparkinsonian medication for at least 2 h, reflecting their typical gait performance during daily activities. All participants underwent clinical assessments, including the H&Y scale and Unified Parkinson's Disease Rating Scale. Physical characteristics, including height, weight, shoulder width, hip and waist circumference, thigh and calf circumference, and leg length, were also measured. Prior to data collection, participants completed a 5-min warm-up consisting of stretching exercises. Static calibration was performed while participants stood still wearing the shoe-type IMU sensors.

Gait assessment was conducted using wearable inertial measurement units under three walking conditions: preferred walking speed (PWS), slower walking speed (SWS; 80% of PWS), and FWS (120% of

PWS). Participants were instructed to walk at their self-defined comfortable pace to determine PWS, which was quantified using a metronome in steps per minute. SWS and FWS were subsequently calculated as 80% and 120% of PWS, respectively. Participants completed three to five practice trials with metronome guidance to adapt to the target walking speeds. Following an adaptation period and a washout phase, all gait trials were performed without auditory cues to avoid potential cueing effects, particularly in individuals with PD.

Gait data were collected along a straight walkway using the same wearable sensor system in both groups. To ensure comparable gait measurements, only steady-state walking segments were included in the analysis. Initial acceleration and terminal deceleration phases (2 m at each end) were excluded, and time-series gait data were extracted from the remaining continuous walking segments. Because the available walkway length differed between experimental environments, the effective steady-state walking distance was approximately 15 m in the fall-prone older adults and 20 m in the PD group.

All sensor data were sampled at 100 Hz and filtered using a second-order Butterworth low-pass filter with a cutoff frequency of 10 Hz. Gait events were identified based on acceleration signals, with heel strikes detected as peaks in anteroposterior acceleration and toe-offs identified as peaks in vertical acceleration. Subsequent gait analyses and image-based representations were derived from stride-normalized segments, minimizing the influence of absolute walking distance.

Signal processing and scalogram image generation

For image-based modeling, one-dimensional inertial sensor signals were segmented using an overlapping sliding-window approach. Given the sampling frequency of 100 Hz, a window length of 1.0 s (100 samples) was applied to each sensor channel, while the window was shifted by 0.5 s (50 samples) between consecutive segments. This configuration generated partially overlapping segments in which each new segment shared 50% of its data with the previous one. The selected window length was designed to capture at least one complete gait cycle during steady walking, since a typical gait cycle in older adults occurs approximately every 1–1.2 s. Meanwhile, the 0.5-s stride provided sufficient temporal resolution to detect gradual changes in gait dynamics while maintaining overlap between segments, which helps stabilize time-series representations and increases the effective number of training samples. Overlapping sliding-window segmentation is widely used in time-series analysis to preserve temporal continuity while improving the robustness of machine-learning models [21]. Using this procedure, each walking trial was decomposed into a sequence of short-duration signal segments representing local gait dynamics.

Sixteen gait-related channels were used for image generation, including tri-axial accelerations and angular velocities from the left and right sensors (L/R X/Y/Z acceleration and gyroscope), as well as their vector magnitudes (L_acc_XYZ, L_gyr_XYZ, R_acc_XYZ, R_gyr_XYZ). These channels were selected to capture bilateral lower-limb kinematics comprehensively while maintaining a fixed and interpretable multi-channel input structure for the convolutional neural network (CNN).

For each segment, a CWT using the Morlet wavelet was applied to generate time–frequency representations of the inertial signals. Wavelet coefficients were computed across scales 1–63 with a sampling period of 1/100 s. The Morlet wavelet was chosen because it provides a suitable balance between temporal and frequency resolution for analyzing non-stationary gait signals. Scalogram power was defined as the squared magnitude of the wavelet coefficients ($|CWT|^2$), representing the signal energy distribution across time and frequency. CWT-based time–frequency representations have been widely used to characterize non-stationary patterns in wearable sensor signals and have demonstrated strong performance as inputs for CNNs in human activity recognition and gait analysis tasks [22–25]. To reduce the influence of extreme values and improve numerical stability during model training, scalogram power values were clipped at the 99th percentile within each segment and subsequently normalized to a 0–1 range. Finally, the normalized scalograms were resized and converted into 128 × 128 RGB images, which served as inputs to the CNN models. Output files were organized hierarchically according to group (PD or fall-prone older adults) and sensor channel, and each image filename encoded the source recording and segment index to preserve temporal ordering.

Model development, validation, and post-processing

Dataset construction

Scalogram images served as inputs to CNNs. For single-channel models, each input consisted of a grayscale scalogram derived from one sensor variable. For multi-channel models, 16 corresponding scalograms were stacked along the channel dimension to form a 128 × 128 × 16 input tensor. Only segments available across all 16 channels for a given subject and segment index were included to ensure consistent input dimensionality.

Subject-wise cross-validation

Model performance was evaluated using subject-wise stratified five-fold cross-validation. StratifiedGroupKFold was used when available, with subject identifiers treated as grouping variables to prevent segments from the same participant from appearing in both training and validation sets. Otherwise, stratified splitting was performed at the subject level. All segment-level samples inherited the diagnostic label of their corresponding subject (PD or fall-prone older adults).

CNN architecture and training

Both single- and multi-channel CNNs employed the same backbone architecture, consisting of sequential two-dimensional convolutional layers with 32, 64, and 128 filters (3 × 3 kernels; ReLU activation; same padding), interleaved with max-pooling layers. Global average pooling was applied prior to a fully connected layer with 128 units (ReLU activation), followed by a sigmoid output layer for binary classification. Models were trained using the Adam optimizer (learning rate 1×10^{-4}) and binary cross-entropy loss for up to 15 epochs with a batch size of 32. To address class imbalance, class weights were

computed using an inverse-frequency balanced scheme and applied during training. Early stopping and learning-rate reduction on a plateau were employed based on validation area under the receiver operating characteristic curve (ROC–AUC), and the best-performing model for each fold was retained.

Performance evaluation and segment-level analysis

For each validation fold, the trained CNN generated probabilistic prediction scores for individual segments. Discriminative performance was evaluated using ROC–AUC. Accuracy was computed using a fixed probability threshold of 0.5 for fold-level descriptive reporting only. ROC curves were generated for each fold, and mean ROC curves with variability across folds were summarized.

All segment-level predictions were exported to CSV files, including subject identifiers, segment indices, predicted scores, and true labels. For the multi-channel model, channel importance was assessed using an occlusion analysis, in which one input channel was set to zero at a time, and the resulting change in AUC (ΔAUC) was quantified.

Post-processing and subject-level decision rules

Operating-point selection

To control false-positive classifications in the fall-prone older adults' group, the primary operating threshold (T_high) was determined from the segment-level ROC curve using a target false-positive rate (FPR) strategy. Specifically, T_high was selected to achieve an FPR of 5% while maximizing sensitivity. A corresponding lower threshold (T_low) was defined as T_high minus a fixed margin ($\Delta = 0.08$), bounded at zero.

Smoothing, hysteresis, and transition detection

Segment-level prediction scores were ordered by segment index and smoothed using a moving average filter with a window size of three segments. A hysteresis-based rule was applied, where entry into a positive (PD-like) state required the smoothed score to exceed T_high for three consecutive segments, and exit required the score to fall below T_low for the same duration. The first transition time was defined as the onset of the first sustained entry into the positive state and converted to seconds using the segment stride (0.5 s).

Dual-rule subject-level classification

Subject-level classification was primarily determined by the presence of a detected transition. In addition, a dual decision rule was applied such that a subject was also classified as positive if the proportion of smoothed segments exceeding T_high (high_ratio) was ≥ 0.05, even in the absence of a detected transition.

Subject-level summary metrics and sensitivity analyses

For each subject, summary metrics were computed, including the total number of segments, mean and maximum prediction scores, proportion of segments exceeding *T*_high (high_ratio), and estimated first transition segment and corresponding time. Subject-level classification performance was evaluated using confusion matrices to derive sensitivity, specificity, accuracy, positive predictive value, negative predictive value, F1 score, and the control over-detection rate.

To minimize potential bias arising from threshold selection, a fold-wise thresholding strategy was implemented as a sensitivity analysis. Within each cross-validation fold, *T*_high was selected using the same target FPR (5%) criterion and applied exclusively to subjects within that fold. Subject-level performance metrics are summarized as mean ± standard deviation across folds.

As an additional sensitivity analysis, the operating-point constraint was relaxed to an upper bound FPR of 10% and compared with the primary 5% operating point using identical post-processing and decision rules. For this analysis, a fixed operating threshold was determined from the overall dataset and applied uniformly across all subjects.

Decision curve analysis

Clinical utility was evaluated using decision curve analysis (DCA) at the subject level, with the mean prediction score used as the decision variable. Net benefit was calculated across threshold probabilities ranging from 0.01 to 0.99 and compared with “treat all” and “treat none” strategies.

Visualization of time-by-channel score patterns

For illustrative purposes, time-by-channel heatmaps were generated for subjects with available single-channel segment-level predictions. These visualizations depicted the temporal evolution of PD-likeness scores across sensor channels, with estimated transition times indicated when applicable. These visualizations were used for exploratory interpretation and were not involved in model training or evaluation. All analyses were conducted using Python 3.10 within a Conda-managed environment with TensorFlow, scikit-learn, NumPy, Pandas, and PyWavelets libraries (Fig. 1).

Statistical Analysis

Data normality was assessed using the Shapiro–Wilk test. Depending on the distribution, either an independent t-test or a non-parametric test was used to compare demographic and clinical characteristics between groups. Agreement between estimated and measured walking speeds was evaluated using intraclass correlation coefficients (ICC) derived from a two-way mixed-effects model for consistency (3,1). The limits of agreement (LoA) between the measured and estimated walking speeds were calculated using the Bland–Altman plot. Statistical analyses were performed using SPSS version 21.0 (IBM Corp., Armonk, NY, USA), with significance set at $p < 0.05$.

Results

Reliability of estimation and measurement speeds

The agreement between target and actual walking speeds showed moderate-to-good reliability in the SWS and good-to-excellent reliability in the FWS across both groups. Specifically, ICC(3,1) values for the SWS were 0.739 in the PD group and 0.801 in the fall-prone older adult group, whereas ICC(3,1) values for the FWS were 0.839 and 0.875, respectively (all $p < 0.001$). These results support the validity of the walking speed protocol used in this study (Table 2, Fig. 2).

Table 2
Reliability of the results for slower and faster walking speeds.

Slower	**PDs (n = 50)**	**Fall-prone older adults (n = 161)**
Estimated/measured (m/s)	0.99/0.94	0.92/0.80
ICC (3,1)	0.739	0.801
p-value	< 0.001	< 0.001
Faster		
Estimated/measured (m/s)	1.48/1.50	1.38/1.44
ICC (3,1)	0.839	0.875
p-value	< 0.001	< 0.001

ICC values were calculated using a two-way mixed-effects model for consistency (ICC(3,1)). Estimated speed represents the target walking speed calculated from preferred walking speed, whereas measured speed represents the actual walking speed recorded during gait assessment. ICC, intraclass correlation coefficient; significant difference, $p < 0.05$.

Segment-level performance of the multi-channel model across walking speeds

At the segment level, the multi-channel CNN demonstrated robust performance in distinguishing PD gait segments from those in fall-prone older adults across different walking speed conditions.

Across FWS, PWS, and SWS, the mean ROC–AUC remained consistently high (FWS: 0.992 ± 0.007; PWS: 0.974 ± 0.016; SWS: 0.975 ± 0.017), indicating reliable PD-likeness prediction irrespective of walking speed (Table 3, Fig. 3). Performance variability across cross-validation folds was low for all speed conditions, supporting the stability and generalizability of the segment-level classification model.

Table 3
Segment-level classification performance of the multi-channel model.

Walking speed	ROC–AUC (mean ± SD)	Accuracy (mean ± SD)
Faster	0.992 ± 0.007	0.953 ± 0.025
Preferred	0.974 ± 0.016	0.921 ± 0.025
Slower	0.975 ± 0.017	0.925 ± 0.023

Classification performance is summarized using the area under the receiver operating characteristic curve (ROC–AUC) and accuracy for faster, preferred, and slower walking conditions. Values are reported as mean ± standard deviation across subject-wise cross-validation folds.

In contrast with the multi-channel model, single-channel models trained on individual sensor-derived inputs demonstrated lower and more variable segment-level classification performance. Across walking speed conditions, representative single-channel models achieved ROC–AUC values in the range of approximately 0.65 to 0.75, with no single variable consistently approaching the performance of the multi-channel model (Supplementary Table S1). These findings highlight the advantage of integrating multi-sensor information for robust PD-likeness prediction at the segment level.

Subject-level transition detection performance

In this study, the term “transition” refers to a model-based subject-level state defined by the proposed post-processing and decision rules, rather than a clinically confirmed longitudinal conversion.

A total of 211 participants were included in the subject-level analysis. The proportion of participants classified as transition cases varied across walking speeds, with 65 (30.8%) under FWS, 52 (24.6%) under PWS, and 54 (25.6%) under SWS. At the subject level, individuals classified as transition cases showed significantly higher mean PD-likeness scores than those classified as non-transition across all walking speed conditions (two-sided Mann–Whitney U tests). Under the FWS, transition subjects demonstrated markedly elevated mean PD-likeness scores relative to non-transition subjects (0.727 ± 0.307 vs. 0.034 ± 0.041, $p < 0.001$). Comparable differences were observed during PWS (0.817 ± 0.210 vs. 0.076 ± 0.077, $p < 0.001$) and SWS (0.787 ± 0.181 vs. 0.084 ± 0.073, $p < 0.001$) (Fig. 4).

Similarly, the proportion of high PD-likeness segments was substantially greater in transition subjects across all walking speeds (FWS: 0.827 ± 0.292 vs. 0.005 ± 0.022; PWS: 0.880 ± 0.216 vs. 0.012 ± 0.038; SWS: 0.865 ± 0.237 vs. 0.006 ± 0.020; all $p < 0.001$) (Table 4). These findings demonstrate that subject-level aggregation of segment-wise PD-likeness predictions robustly distinguishes subjects classified as transition cases from those classified as non-transition, regardless of walking speed.

Table 4
Subject-level high PD-likeness ratio.

Walking speed	Transition (mean ± SD)	Non-transition (mean ± SD)	p-value
Faster	0.827 ± 0.292	0.005 ± 0.022	< 0.001
Preferred	0.880 ± 0.216	0.012 ± 0.038	< 0.001
Slower	0.865 ± 0.237	0.006 ± 0.020	< 0.001

The table summarizes the proportion of segments exceeding the high PD-likeness threshold (high_ratio) for subjects classified as transition and non-transition cases under faster, preferred, and slower walking conditions. Values are presented as mean ± standard deviation. Group differences are assessed using two-sided Mann–Whitney U tests. PD, Parkinson's disease.

Temporal characteristics of PD-like transition

To characterize the temporal dynamics of PD-like gait emergence, we examined the timing of the first sustained high PD-likeness segment among transition subjects. Across all walking speed conditions, sustained PD-like segments emerged early during the walking task, with a median first transition time of approximately 0.5 s. This early onset pattern was consistently observed under FWS, PWS, and SWS, indicating that the temporal emergence of PD-like gait characteristics was not dependent on walking speed.

Sensitivity/robustness analyses

Fold-wise stability

Under fold-wise threshold selection, subject-level classification performance remained stable across cross-validation folds. For the PWS, accuracy was 0.910 ± 0.062, with sensitivity of 0.98 ± 0.045 and specificity of 0.888 ± 0.082. Comparable stability was observed under FWS (accuracy: 0.891 ± 0.054) and SWS (accuracy: 0.924 ± 0.054). These findings indicate that subject-level transition detection performance was not driven by a specific fold (Table 5).

Table 5
Fold-wise subject-level performance (5% FPR)

Walking speed	Accuracy (mean ± SD)	Sensitivity (mean ± SD)	Specificity (mean ± SD)	F1 score (mean ± SD)
Faster	0.891 ± 0.054	1.00 ± 0.00	0.857 ± 0.071	0.819 ± 0.082
Preferred	0.910 ± 0.062	0.98 ± 0.045	0.888 ± 0.082	0.845 ± 0.087
Slower	0.924 ± 0.054	1.00 ± 0.00	0.900 ± 0.071	0.869 ± 0.085

Subject-level classification performance of the multi-channel model is summarized across walking speed conditions using subject-wise cross-validation folds. Performance metrics include accuracy, sensitivity, specificity, and F1 score. Values are reported as mean ± standard deviation across folds. The operating threshold is determined to achieve a target false-positive rate of 5%. FPR, false-positive rate.

Operating-point sensitivity (5% vs. 10% FPR)

To further evaluate the robustness of the model to threshold selection, we compared performance under different operating-point constraints using a fixed threshold derived from the overall dataset. This analysis complements the fold-wise thresholding approach presented above, in which thresholds were determined independently within each cross-validation fold.

Relaxing the operating-point constraint from a target FPR of 5% to 10% resulted in a modest increase in sensitivity but a substantial reduction in specificity across walking speed conditions. Under the PWS, sensitivity increased from 0.96 to 0.98, whereas specificity decreased from 0.882 to 0.727, leading to a reduction in overall accuracy (0.900 to 0.787). Similar patterns were observed under FWS and SWS. These findings indicate that a conservative 5% FPR provides a more balanced trade-off between sensitivity and specificity while maintaining robust performance (Table 6).

Table 6
Subject-level performance under different operating-point constraints.

Walking speed	FPR target	Sensitivity	Specificity	Accuracy
Faster	5%	1.00	0.857	0.891
Faster	10%	1.00	0.689	0.763
Preferred	5%	0.96	0.882	0.900
Preferred	10%	0.98	0.727	0.787
Slower	5%	1.00	0.913	0.934
Slower	10%	1.00	0.752	0.810

Subject-level sensitivity, specificity, and accuracy of the multi-channel model are reported for operating thresholds corresponding to target false-positive rates of 5% and 10% across walking speed conditions.

Decision curve analysis

DCA demonstrated that the multi-channel model provided a positive net benefit across threshold probabilities ranging approximately from 0.05 to 0.60 under FWS, PWS, and SWS. Across this clinically relevant range, the model consistently outperformed both treat-all and treat-none strategies, supporting the potential clinical utility of subject-level PD transition detection (Fig. 5).

Discussion

In this study, we developed and validated a multi-channel deep learning framework that can identify PD-like motor states and detect transition events using segment-level gait-derived time–frequency representations from wearable inertial sensors. Three principal findings emerged. First, the multi-channel model demonstrated substantially superior discriminative performance compared with single-channel approaches. Second, segment-level temporal modeling enabled detection of sustained PD-like motor patterns through high-resolution probability trajectories. Third, transition-related metrics derived from segment aggregation provided interpretable indicators of PD-like motor phenotype expression at the subject level.

Multi-channel integration improves detection of parkinsonian gait dynamics

Our results demonstrate that integrating multi-sensor inertial signals within a time–frequency deep learning framework markedly improves discrimination of PD-like gait dynamics compared with single-channel approaches [19, 20, 26]. The multi-channel CNN achieved near-ceiling segment-level performance across walking speeds (ROC–AUC up to 0.992), whereas individual sensor-derived inputs yielded substantially lower and more variable performance [19, 26]. These findings suggest that PD-related motor alterations are not confined to isolated axes or single limbs but instead reflect disruptions in coordinated, multi-planar, and bilateral motor integration [16, 27, 28]. By simultaneously modeling cross-axis synchrony and inter-limb dynamics, the multi-channel architecture captured integrated motor signatures that single-channel models were unable to detect [19, 26].

From a motor control perspective, parkinsonian motor impairment is characterized by increased gait asymmetry, impaired trunk–lower limb coupling, and reduced movement automaticity—features arising from dysfunction within distributed corticobasal ganglia–brainstem motor networks [16, 27, 29]. By integrating bilateral accelerometer axes, gyroscope axes, and composite magnitude features, the present model likely captured coordinated spatiotemporal and oscillatory abnormalities rather than isolated signal deviations [16, 26, 27]. Thus, the superiority of the multi-channel architecture likely reflects improved modeling of motor system integration breakdown rather than a simple increase in feature dimensionality [16, 28].

Segment-level modeling enables detection of dynamic motor-state transitions

Building upon this high-resolution segment-level modeling, we implemented a conservative hysteresis-based framework to identify sustained entry into PD-like motor states at the subject level [20, 30]. Using a predefined operating threshold corresponding to a 5% FPR and requiring three consecutive high-probability segments for state entry, the model achieved high sensitivity (0.96–1.00) while maintaining strong specificity (0.857–0.913) across walking speeds [30, 31]. This design prioritized stability over transient fluctuations and minimized over-detection in non-PD individuals.

Importantly, the transition detected in this study represents entry into a sustained PD-like motor phenotype, rather than clinical diagnostic conversion to PD [16, 26]. Instead of relying solely on static subject-level classification, the present framework captures dynamic probability trajectories across time [30, 32]. This distinction is important because PD motor deterioration is generally not abrupt but gradually accumulates through subtle fluctuations in movement variability, jerk modulation, and coordination instability [9, 16]. Traditional analyses based on averaged gait parameters may dilute such micro-level fluctuations [9, 32]. In contrast, segment-level modeling enables detection of transient PD-like patterns that would likely be obscured under subject-level averaging approaches [30, 32]. These findings support a micro-instability hypothesis, whereby early transition toward a PD-like motor phenotype may initially manifest as increased intra-individual variability rather than uniform motor impairment [9, 33].

Walking speed as a functional stressor revealing latent motor deficits

An additional finding of this study was that segment-level discriminative performance remained consistently high across walking speeds, with the highest performance observed during FWS. This observation is consistent with prior gait studies showing that locomotor task demands modulate the detectability of parkinsonian motor abnormalities [9, 34]. The speed-dependent pattern may have mechanistic relevance rather than reflecting a purely methodological effect, since gait speed is recognized as an important modulator of neural control strategies during locomotion [16].

FWS imposes greater demands on motor automaticity, inter-limb coordination, and dynamic postural stability—processes strongly dependent on basal ganglia–mediated locomotor regulation [34, 35]. Previous studies have shown that individuals with parkinsonian motor impairment experience disproportionate difficulty maintaining rhythmic coordination and gait stability as walking speed increases, leading to amplified stride variability and reduced adaptability of movement patterns [9, 36, 37].

From a motor control perspective, FWS reduces the opportunity for conscious compensatory strategies and increases reliance on automatic locomotor programs governed by subcortical networks [16, 38]. Because PD-related dysfunction primarily affects automatic movement regulation, pathological motor signatures may become more pronounced under higher-speed locomotor conditions [34, 39]. Consequently, PD-like gait dynamics may be more readily distinguishable from non-PD gait during FWS, explaining the superior discriminative performance observed in this condition [9, 40].

Importantly, the preservation of strong performance across PWS and SWS indicates that PD-like motor instability is not restricted to a specific locomotor state but represents a stable motor phenotype observable across functional contexts [30, 40]. Together, these findings support the concept that gait speed may function as a physiological stressor that reveals latent locomotor control deficits, consistent with frameworks proposing that increased motor demand exposes subclinical motor impairments in parkinsonian populations [10, 16].

Clinical implications for fall-prone older adults

The clinical relevance of these findings is particularly notable in older adults with a history of falls [41, 42]. Falls in aging populations are associated with increased gait variability, impaired postural reflexes, reduced automaticity, and executive dysfunction—features that overlap with early parkinsonian motor characteristics [16, 33, 42]. The markedly elevated proportion of high PD-likeness segments among transition-positive individuals suggests that, in a subset of fall-experienced older adults, motor instability may reflect PD-like motor network vulnerability rather than generalized age-related frailty alone [26, 32, 42]. In this context, the proposed framework may provide a quantitative approach for motor risk stratification within clinically vulnerable populations, potentially supporting earlier identification of individuals exhibiting parkinsonian-like motor phenotypes [30, 42]. This may be particularly relevant for developing individualized monitoring and mobility management strategies in older adults with recurrent falls.

Methodological considerations

An important methodological consideration of this study is the difference in age thresholds between the PD and fall-prone older adult groups [26, 43]. Individuals with PD were included from 50 years of age to reflect the typical onset range of idiopathic PD, whereas the fall-prone group was restricted to adults aged 65 years or older with a history of falls to represent a population with substantial age-related functional vulnerability [26, 41, 43]. This design intentionally created a conservative comparison framework, evaluating PD-related gait characteristics against an older high-risk non-PD population rather than younger healthy controls [26, 41, 43]. Although the deep-learning models did not explicitly include chronological age as a covariate, age-related motor characteristics were implicitly embedded within the learned spatiotemporal gait representations [19, 43]. Therefore, classification performance likely reflects integrated gait signatures rather than chronological age alone [26, 43]. Future studies with larger cohorts may benefit from age-stratified or age-matched analyses to further disentangle disease-specific gait patterns from aging-related changes [26, 43]. Additionally, although analyzed walking distances differed between groups, the use of stride-normalized and image-based representations minimized the effect of absolute walking distance on model learning, thereby reducing potential bias associated with task duration differences [20, 44].

Comparison with previous approaches

Compared with previous studies that primarily relied on summary gait parameters, subject-level cross-sectional classification, or clinical score–based binary modeling, the present study employed time-series imaging of gait signals, segment-level deep learning, and probability trajectory analysis [19, 20, 26]. By modeling locomotor signals at high temporal resolution, this framework enables dynamic estimation of PD-like probability over time, providing both mechanistic insight and clinically interpretable state transitions [9, 20, 30]. Beyond discrimination accuracy, DCA demonstrated positive net benefit across clinically relevant threshold probabilities (approximately 0.05–0.60), suggesting that the model may offer

practical value for identifying higher-risk motor phenotypes among fall-experienced older adults compared with treat-all or treat-none strategies [31].

Strengths and limitations

This study has several notable strengths. Integration of 16 synchronized inertial sensor channels enabled comprehensive modeling of bilateral lower-limb kinematics within a unified time–frequency deep-learning framework [17, 19]. Conservative operating-point selection (5% FPR), hysteresis-based transition rules, temporal smoothing, and fold-wise threshold sensitivity analyses collectively enhanced analytical robustness [30, 31]. Furthermore, the incorporation of DCA extended evaluation beyond statistical discrimination to clinical utility [31].

Some limitations should also be acknowledged. The detected transition represents a model-defined PD-like motor state rather than longitudinal clinical conversion to PD [16, 31]. The cross-sectional single-session design precludes direct inference regarding future diagnostic outcomes [26, 41]. External validation in independent cohorts will be necessary to confirm the generalizability of the framework [17, 19]. In addition, although CNNs provide powerful pattern recognition capabilities, the interpretability of learned representations remains limited [45, 46]. Future work integrating explainable artificial intelligence approaches may improve the mechanistic interpretability of model-derived motor signatures. Importantly, longitudinal studies linking model-defined motor transitions to clinically confirmed PD diagnosis, as well as integration with cognitive, neurophysiological, and imaging biomarkers, represent important next steps [16, 31]. Such efforts may further clarify the potential utility of model-derived motor transitions for longitudinal functional monitoring and intervention tracking.

Conclusions

In this study, we developed and validated a multi-channel time–frequency deep-learning framework capable of identifying parkinsonian gait dynamics at the segment level and summarizing these dynamics into subject-level transition metrics. By leveraging synchronized multi-sensor inertial signals and high-resolution temporal modeling, the proposed approach enabled the detection of sustained PD-like motor states that are not readily observable using conventional subject-level averaging strategies.

Robust performance was maintained across walking speeds while preserving a favorable balance between sensitivity and specificity under a conservative false-positive operating point. Notably, FWS enhanced discriminability, supporting the interpretation that increased locomotor demand acts as a functional stressor, revealing latent motor control deficits associated with parkinsonian pathology.

These findings provide a quantitative basis for identifying parkinsonian-like motor phenotypes within an aging, fall-prone population and establish a foundation for scalable motor risk stratification using wearable sensing technologies. These capabilities may contribute to earlier detection of mobility-related decline and support more personalized management approaches in high-risk older adults. Importantly,

the detected transitions represent model-defined motor states rather than clinical diagnostic conversion. Future longitudinal studies integrating clinical follow-up and multimodal biomarkers will be essential to determine whether these model-derived PD-like states are prospectively associated with clinically confirmed PD outcomes and longitudinal mobility-related functional changes.

Abbreviations

PD
Parkinson’s disease
CWT
Continuous wavelet transforms
FWS
Faster walking speed
H&Y
Hoehn and Yahr
IRB
Institutional Review Board
IMUs
Inertial measurement units
PWS
Preferred walking speed
SWS
Slower walking speed
CNN
Convolutional neural network
ROC–AUC
Area under the receiver operating characteristic curve
FPR
False-positive rate
DCA
Decision curve analysis
ICC
Intraclass correlation coefficients
LoA
Limits of agreement.

Declarations

Ethics approval and consent to participate

All procedures involving human participants were conducted in accordance with the ethical standards of the institutional and/or national research committee and the 1964 Declaration of Helsinki and its later amendments or comparable ethical standards. The study protocol and supplementary materials were approved by the Institutional Review Board of Dong-A University Hospital (Approval No. DAUHIRB-22-089). All participants provided written informed consent prior to data collection. The study was also registered with the Clinical Research Information Service of the Republic of Korea (KCT0009353).

Consent for publication

Not applicable.

Competing interests

The authors declare that they have no competing interests.

Funding

This work was supported by grants from the National Research Foundation of Korea (NRF), funded by the Korean government (MSIT) (no. 2022R1A2C100933711; Changhong Youm); the Basic Science Research Program through the NRF, funded by the Ministry of Education (no. 2022R1A6A3A0108756411; Hwayoung Park); the Ministry of Education of the Republic of Korea and the NRF (no. 2024S1A5B5A16021673; Hwayoung Park); and the Ministry of Education of the Republic of Korea and the National Research Foundation of Korea.(NRF-2025S1A5B5A16007988; Bohyun Kim). This study received no specific grants from funding agencies in the public, commercial, or non-profit sectors. The funding sources had no role in the study design, data collection, analysis, interpretation, or manuscript writing.

Author Contribution

B.K., C.Y., and S.C. conceived and designed the study. B.K., S.C., and H.P. recruited the participants. B.K., C.Y., S.C., H.P., J.H., and M.K. performed data acquisition. B.K. and C.Y. analyzed and interpreted the data. B.K., C.Y., and S.C. drafted the manuscript. All authors reviewed and approved the final version of the manuscript.

Acknowledgement

The authors thank all participants who contributed to this study. This work was supported by the Dong-A University research fund.

Data Availability

The datasets supporting the findings of this study are available from the corresponding author upon reasonable request.

Code availability

The analysis pipeline was implemented in a Conda-managed Python 3.10.18 environment. Deep learning models were developed using TensorFlow CPU 2.19.1 and Keras 3.11.2. Subject-wise cross-validation, classification performance evaluation, and statistical metrics were implemented using scikit-learn 1.1.3. Data preprocessing and numerical computations were performed using pandas 2.2.3, NumPy 1.26.4, and SciPy 1.15.3. Continuous wavelet transform–based scalogram generation was implemented using PyWavelets 1.8.0. Image processing and input handling were performed using Pillow 11.1.0. Figures and visualizations were generated using Matplotlib 3.10.0 and Seaborn 0.13.2. Excel file input/output operations were performed using openpyxl 3.1.5. The analysis code is not publicly available because of data privacy and intellectual property considerations, but may be made available from the corresponding author upon reasonable request for academic purposes.

References

1. Kalia LV, Lang AE. Parkinson's disease. Lancet. 2015;386(9996):896–912. 10.1016/S0140-6736(14)61393-3.
2. Maetzler W, Mirelman A, Pilotto A, Bhidayasiri R. Identifying Subtle Motor Deficits Before Parkinson's Disease is Diagnosed: What to Look for? J Parkinsons Dis. 2024;14(s2):S287–96. 10.3233/JPD-230350.
3. Postuma RB, Berg D, Stern M, et al. MDS clinical diagnostic criteria for Parkinson's disease. Mov Disord. 2015;30(12):1591–601. 10.1002/mds.26424.
4. Mancini M, Afshari M, Almeida Q, et al. Digital gait biomarkers in Parkinson's disease: susceptibility/risk, progression, response to exercise, and prognosis. NPJ Parkinsons Dis. 2025;11(1):51. 10.1038/s41531-025-00897-1.
5. Berg D, Postuma RB, Adler CH, et al. MDS research criteria for prodromal Parkinson's disease. Mov Disord. 2015;30(12):1600–11. 10.1002/mds.26431.
6. Postuma RB, Iranzo A, Hu M, et al. Risk and predictors of dementia and parkinsonism in idiopathic REM sleep behaviour disorder: a multicentre study. Brain. 2019;142(3):744–59. 10.1093/brain/awz030.
7. Camacho-Soto A, Warden MN, Searles Nielsen S, et al. Traumatic brain injury in the prodromal period of Parkinson's disease: A large epidemiological study using medicare data. Ann Neurol. 2017;82(5):744–54. 10.1002/ana.25074.

8. Nyström H, Nordström A, Nordström P. Risk of Injurious Fall and Hip Fracture up to 26 y before the Diagnosis of Parkinson Disease: Nested Case-Control Studies in a Nationwide Cohort. PLoS Med. 2016;13(2):e1001954. 10.1371/journal.pmed.1001954.
9. Hausdorff JM. Gait dynamics in Parkinson's disease: common and distinct behavior among stride length, gait variability, and fractal-like scaling. Chaos. 2009;19(2):026113. 10.1063/1.3147408.
10. Yogev-Seligmann G, Hausdorff JM, Giladi N. The role of executive function and attention in gait. Mov Disord. 2008;23(3):329–472. 10.1002/mds.21720.
11. Salari N, Darvishi N, Ahmadipanah M, Shohaimi S, Mohammadi M. Global prevalence of falls in the older adults: a comprehensive systematic review and meta-analysis. J Orthop Surg Res. 2022;17(1):334. 10.1186/s13018-022-03222-1.
12. Kearney FC, Harwood RH, Gladman JR, Lincoln N, Masud T. The relationship between executive function and falls and gait abnormalities in older adults: a systematic review. Dement Geriatr Cogn Disord. 2013;36(1–2):20–35. 10.1159/000350031.
13. Lindholm B, Hagell P, Odin P, et al. Balance and gait disorders in de novo Parkinson's disease: support for early rehabilitation. J Neurol. 2024;272(1):11. 10.1007/s00415-024-12804-4.
14. Jung YJ, Kim R, Yoo D, Han K, Lee JY. Late-life falling and depressive symptoms associated with the risk of Parkinson's disease: a nationwide cohort data analysis. BMC Geriatr. 2020;20(1):284. 10.1186/s12877-020-01691-9.
15. Bradley M, O'Loughlin S, Donlon E, et al. Determining Falls Risk in People with Parkinson's Disease Using Wearable Sensors: A Systematic Review. Sens (Basel). 2025;25(13):4071. 10.3390/s25134071.
16. Peterson DS, Horak FB. Neural Control of Walking in People with Parkinsonism. Physiol (Bethesda). 2016;31(2):95–107. 10.1152/physiol.00034.2015.
17. Prisco G, Pirozzi MA, Santone A, et al. Validity of Wearable Inertial Sensors for Gait Analysis: A Systematic Review. Diagnostics (Basel). 2024;15(1):36. 10.3390/diagnostics15010036.
18. Shokrpour S, MoghadamFarid A, Bazzaz Abkenar S, Haghi Kashani M, Akbari M, Sarvizadeh M. Machine learning for Parkinson's disease: a comprehensive review of datasets, algorithms, and challenges. NPJ Parkinsons Dis. 2025;11(1):187. 10.1038/s41531-025-01025-9.
19. Franco A, Russo M, Amboni M, et al. The Role of Deep Learning and Gait Analysis in Parkinson's Disease: A Systematic Review. Sens (Basel). 2024;24(18):5957. 10.3390/s24185957.
20. Shi B, Yen SC, Tay A, Tan DML, Chia NSY, Au WL. Convolutional Neural Network for Freezing of Gait Detection Leveraging the Continuous Wavelet Transform on Lower Extremities Wearable Sensors Data. Annu Int Conf IEEE Eng Med Biol Soc. 2020;2020:5410–5. 10.1109/EMBC44109.2020.9175687.
21. Wang C, Li X, Zhou T, Cai Z. Unsupervised Time Series Segmentation: A Survey on Recent Advances. Comput Mater Contin. 2024;80(2):2657–73. 10.32604/cmc.2024.054061.
22. Torrence C, Compo GP. A practical guide to wavelet analysis. Bull Amer Meteor Soc. 1998;79(1):61–78. 10.1175/1520-0477(1998)079%3C0061:APGTWA%3E2.0.CO;2.

23. Ahmed N, Numan MOA, Kabir R, Islam MR, Watanobe Y. A Robust Deep Feature Extraction Method for Human Activity Recognition Using a Wavelet Based Spectral Visualisation Technique. Sens (Basel). 2024;24(13):4343. 10.3390/s24134343.
24. Pavliuk O, Mishchuk M, Strauss C. Transfer Learning Approach for Human Activity Recognition Based on Continuous Wavelet Transform. Algorithms. 2023;16(2):77. 10.3390/a16020077.
25. Nedorubova A, Kadyrova A, Khlyupin A. Human activity recognition using continuous wavelet transform and convolutional neural networks. *arXiv preprint arXiv:2106.12666*. 2021. 10.48550/arXiv.2106.12666
26. Zhang W, Ling Y, Chen Z, et al. Wearable sensor-based quantitative gait analysis in Parkinson's disease patients with different motor subtypes. NPJ Digit Med. 2024;7(1):169. 10.1038/s41746-024-01163-z.
27. Fling BW, Curtze C, Horak FB. Gait Asymmetry in People With Parkinson's Disease Is Linked to Reduced Integrity of Callosal Sensorimotor Regions. Front Neurol. 2018;9:215. 10.3389/fneur.2018.00215.
28. Magrinelli F, Picelli A, Tocco P, et al. Pathophysiology of Motor Dysfunction in Parkinson's Disease as the Rationale for Drug Treatment and Rehabilitation. Parkinsons Dis. 2016;2016:9832839. 10.1155/2016/9832839.
29. Galvan A, Wichmann T. Pathophysiology of parkinsonism. Clin Neurophysiol. 2008;119(7):1459–74. 10.1016/j.clinph.2008.03.017.
30. Weiss A, Herman T, Giladi N, Hausdorff JM. Objective assessment of fall risk in Parkinson's disease using a body-fixed sensor worn for 3 days. PLoS ONE. 2014;9(5):e96675. 10.1371/journal.pone.0096675.
31. Vickers AJ, Elkin EB. Decision curve analysis: a novel method for evaluating prediction models. Med Decis Mak. 2006;26(6):565–74. 10.1177/0272989X06295361.
32. Chau T, Young S, Redekop S. Managing variability in the summary and comparison of gait data. J Neuroeng Rehabil. 2005;2:22. 10.1186/1743-0003-2-22.
33. Schaafsma JD, Giladi N, Balash Y, Bartels AL, Gurevich T, Hausdorff JM. Gait dynamics in Parkinson's disease: relationship to Parkinsonian features, falls and response to levodopa. J Neurol Sci. 2003;212(1–2):47–53. 10.1016/s0022-510x(03)00104-7.
34. Morris ME, Iansek R, Matyas TA, Summers JJ. The pathogenesis of gait hypokinesia in Parkinson's disease. Brain. 1994;117(Pt5):1169–81. 10.1093/brain/117.5.1169.
35. Takakusaki K. Functional Neuroanatomy for Posture and Gait Control. J Mov Disord. 2017;10(1):1–17. 10.14802/jmd.16062.
36. Frenkel-Toledo S, Giladi N, Peretz C, Herman T, Gruendlinger L, Hausdorff JM. Effect of gait speed on gait rhythmicity in Parkinson's disease: variability of stride time and swing time respond differently. J Neuroeng Rehabil. 2005;2:23. 10.1186/1743-0003-2-23.
37. Yogev G, Plotnik M, Peretz C, Giladi N, Hausdorff JM. Gait asymmetry in patients with Parkinson's disease and elderly fallers: when does the bilateral coordination of gait require attention? Exp Brain

Res. 2007;177(3):336–46. 10.1007/s00221-006-0676-3.
38. Wu T, Hallett M. A functional MRI study of automatic movements in patients with Parkinson's disease. Brain. 2005;128(Pt 10):2250–9. 10.1093/brain/awh569.
39. Redgrave P, Rodriguez M, Smith Y, et al. Goal-directed and habitual control in the basal ganglia: implications for Parkinson's disease. Nat Rev Neurosci. 2010;11(11):760–72. 10.1038/nrn2915.
40. Del Din S, Godfrey A, Galna B, Lord S, Rochester L. Free-living gait characteristics in ageing and Parkinson's disease: impact of environment and ambulatory bout length. J Neuroeng Rehabil. 2016;13(1):46. 10.1186/s12984-016-0154-5.
41. Beck Jepsen D, Robinson K, Ogliari G, et al. Predicting falls in older adults: an umbrella review of instruments assessing gait, balance, and functional mobility. BMC Geriatr. 2022;22(1):615. 10.1186/s12877-022-03271-5.
42. Bloem BR, Hausdorff JM, Visser JE, Giladi N. Falls and freezing of gait in Parkinson's disease: a review of two interconnected, episodic phenomena. Mov Disord. 2004;19(8):871–84. 10.1002/mds.20115.
43. Menz HB, Lord SR, Fitzpatrick RC. Age-related differences in walking stability. Age Ageing. 2003;32(2):137–42. 10.1093/ageing/32.2.137.
44. Forner-Cordero A. Human gait, stumble and… fall? Mechanical limitations of the recovery from a stumble. 2003..
45. Sujatha Ravindran A, Contreras-Vidal J. An empirical comparison of deep learning explainability approaches for EEG using simulated ground truth. Sci Rep. 2023;13(1):17709. 10.1038/s41598-023-43871-8.
46. Resta M, Monreale A, Bacciu D. Occlusion-Based Explanations in Deep Recurrent Models for Biomedical Signals. Entropy (Basel). 2021;23(8):1064. 10.3390/e23081064.

Figures

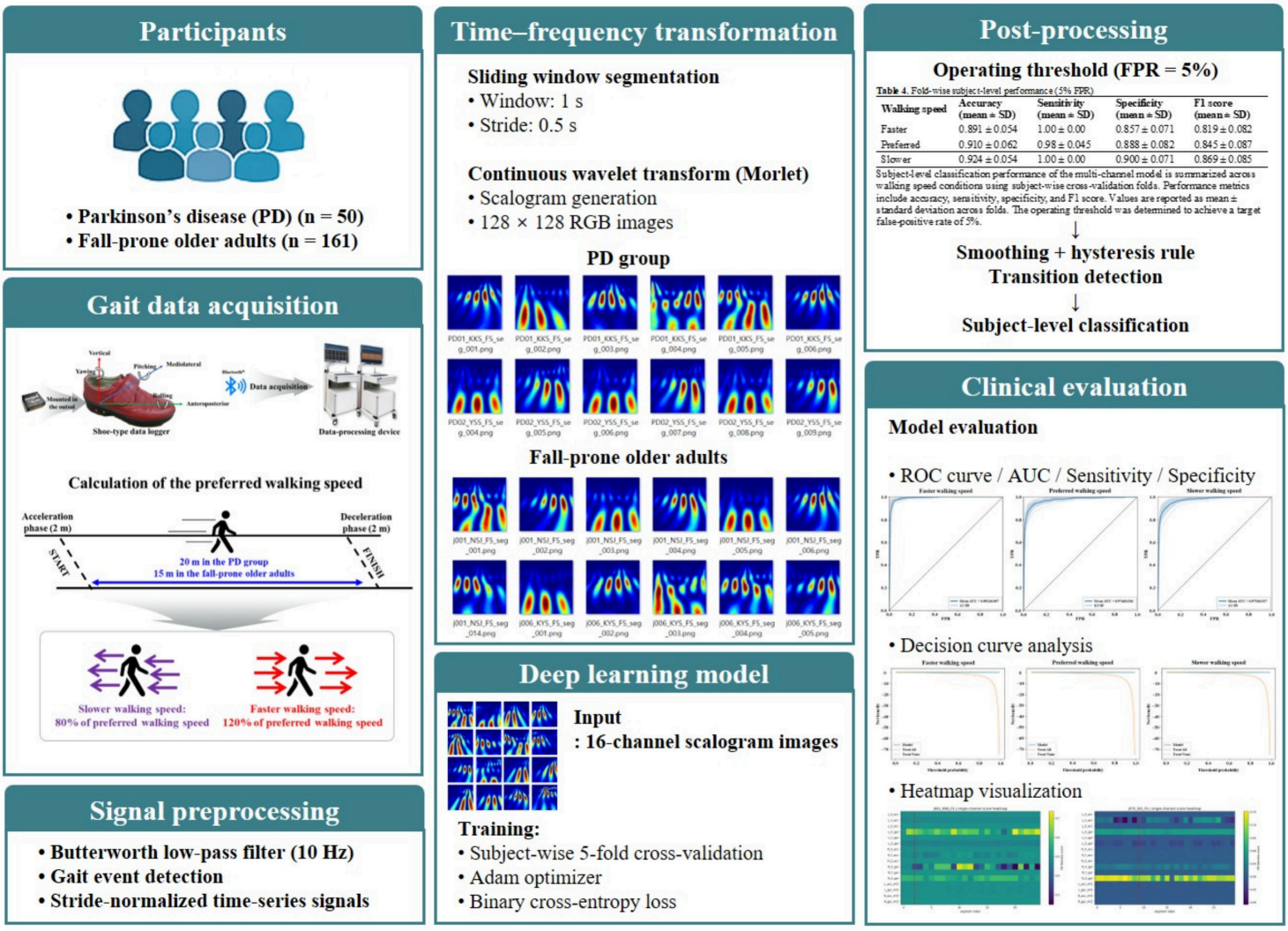


Figure 1

Overview of the proposed analysis pipeline. Gait signals acquired using wearable inertial measurement units are segmented into short time windows and transformed into time–frequency scalogram images using continuous wavelet transform. The scalograms are used as inputs to convolutional neural networks trained using subject-wise cross-validation. Segment-level prediction scores are subsequently processed using threshold-based smoothing and hysteresis rules to detect Parkinson's disease (PD)-like gait transitions and derive subject-level classifications. FPR, false-positive rate; ROC, receiver operating characteristic; AUC, area under the curve.

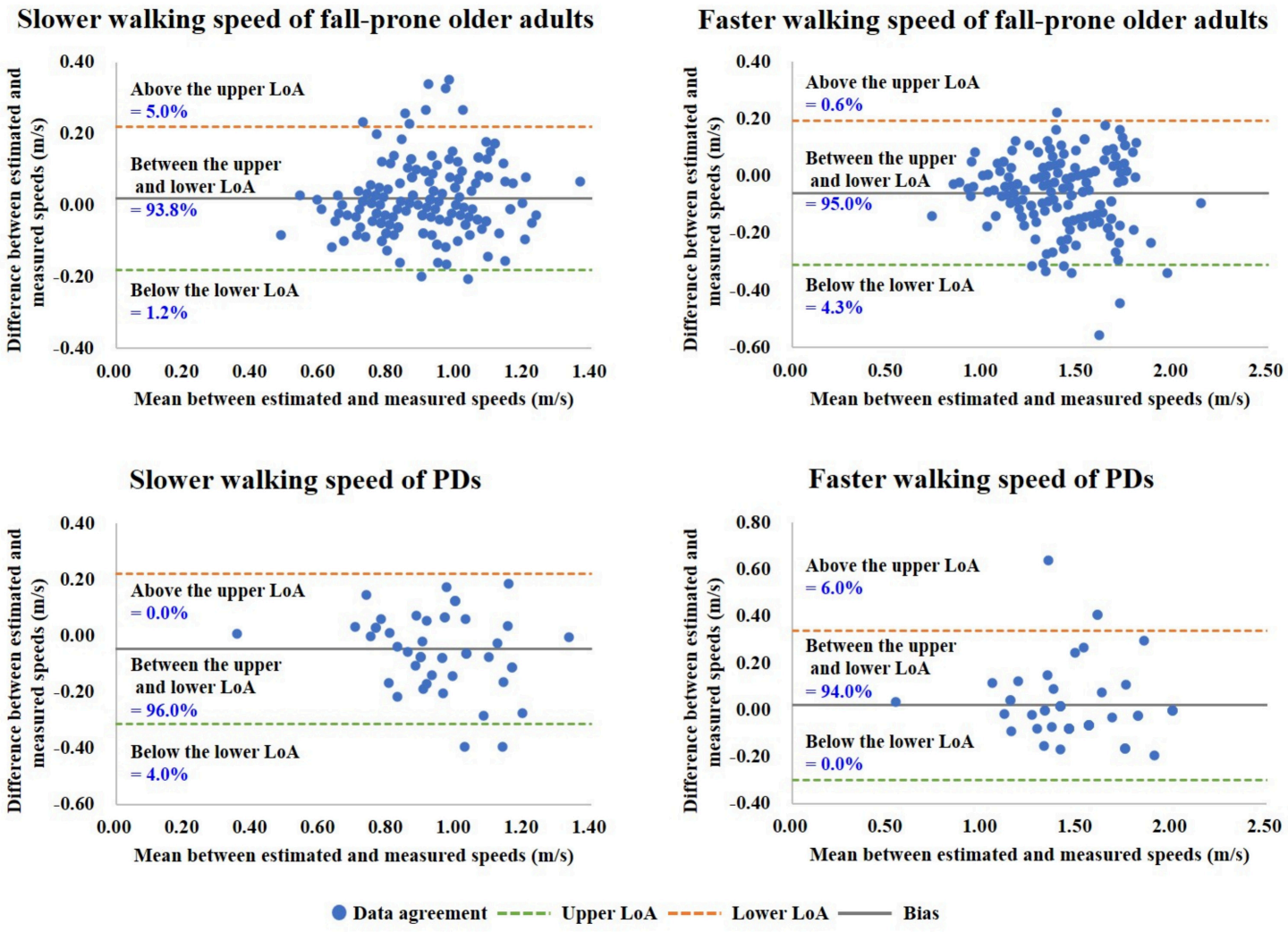


Figure 2

Bland–Altman plots showing agreement between estimated and measured walking speeds under slower and faster walking conditions in fall-prone older adults and patients with Parkinson's disease (PD). The x-axis represents the mean of the estimated and measured walking speeds, whereas the y-axis represents the difference between the two measurements. The solid gray line indicates the mean bias, and the dashed lines represent the upper and lower limits of agreement (LoA; mean difference ± 1.96 standard deviations). Percentages indicate the proportion of participants located above the upper LoA, within the LoA, and below the lower LoA. Most data points were distributed within the LoA across both walking conditions and groups, indicating acceptable agreement between target and actual walking speeds. LoA, limits of agreement.

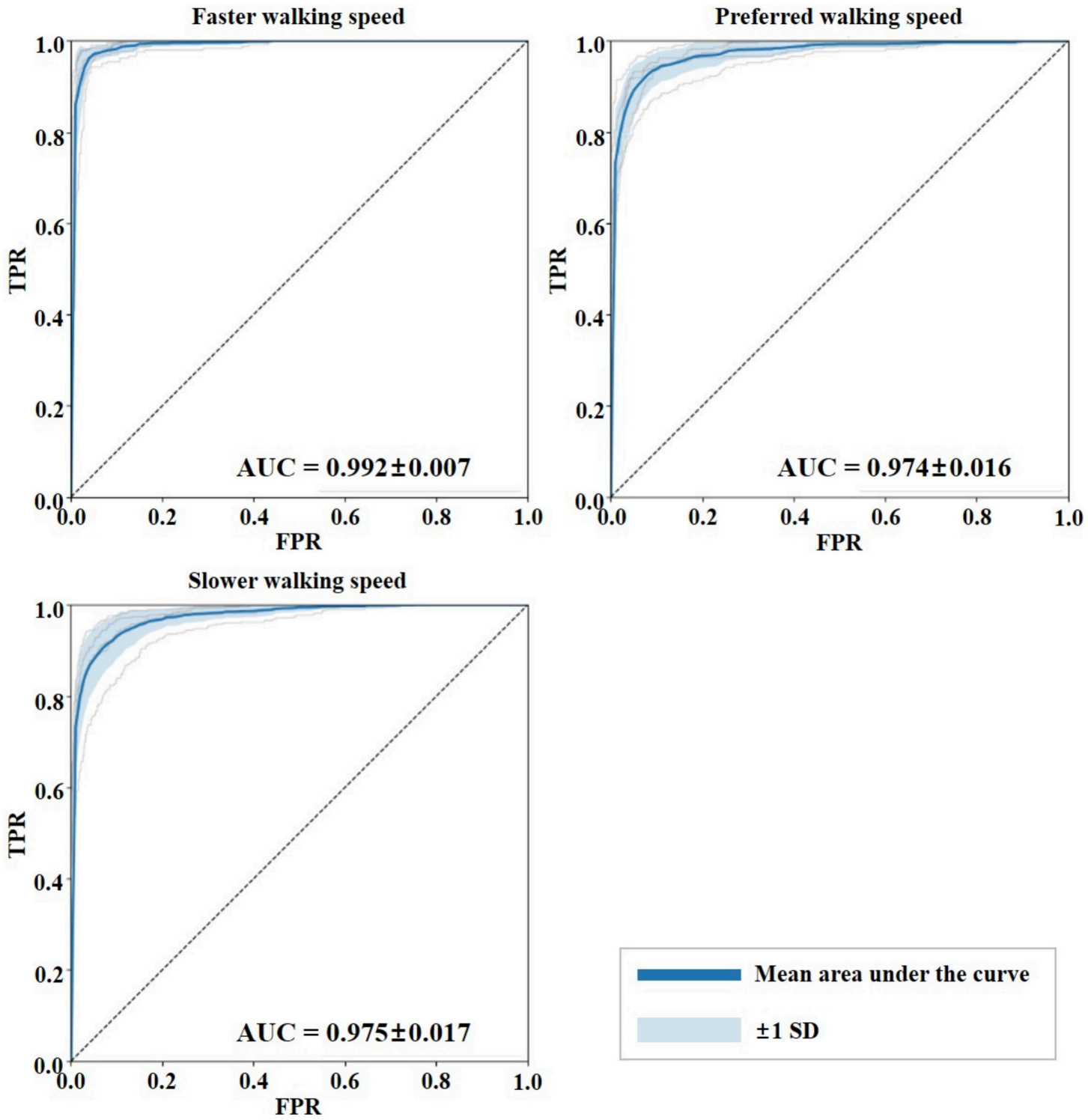


Figure 3

ROC curve of the multi-channel convolutional neural network for segment-level classification of patients with Parkinson's disease versus fall-prone older adults' gait segments. The solid line represents the mean ROC curve across cross-validation folds, and the shaded area indicates ±1 standard deviation, demonstrating robust and stable classification performance. ROC, receiver operating

characteristic; AUC, area under the curve; TPR, true positive rate; FPR, false-positive rate; SD, standard deviation.

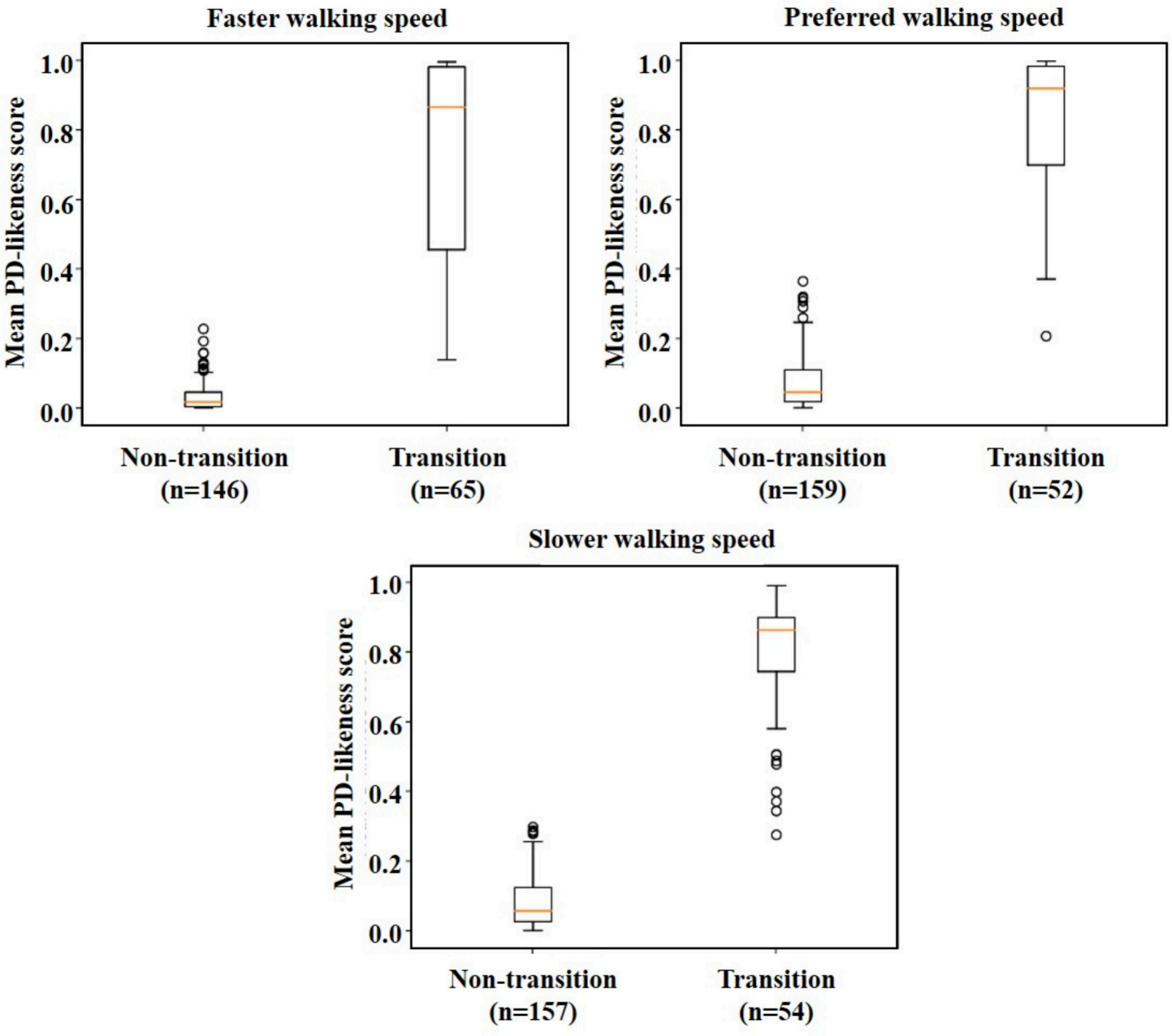


Figure 4

Subject-level mean Parkinson's disease (PD)-likeness scores in transition and non-transition groups across walking speed conditions. Boxplots represent the distribution of mean PD-likeness scores under faster, preferred, and slower walking conditions. Transition subjects exhibit significantly higher mean PD-likeness scores than non-transition across all walking speeds. Group differences were evaluated using two-sided Mann–Whitney U tests (all $p < 0.001$). Boxes indicate the interquartile range, center lines represent medians, whiskers denote 1.5× interquartile range, and circles indicate outliers.

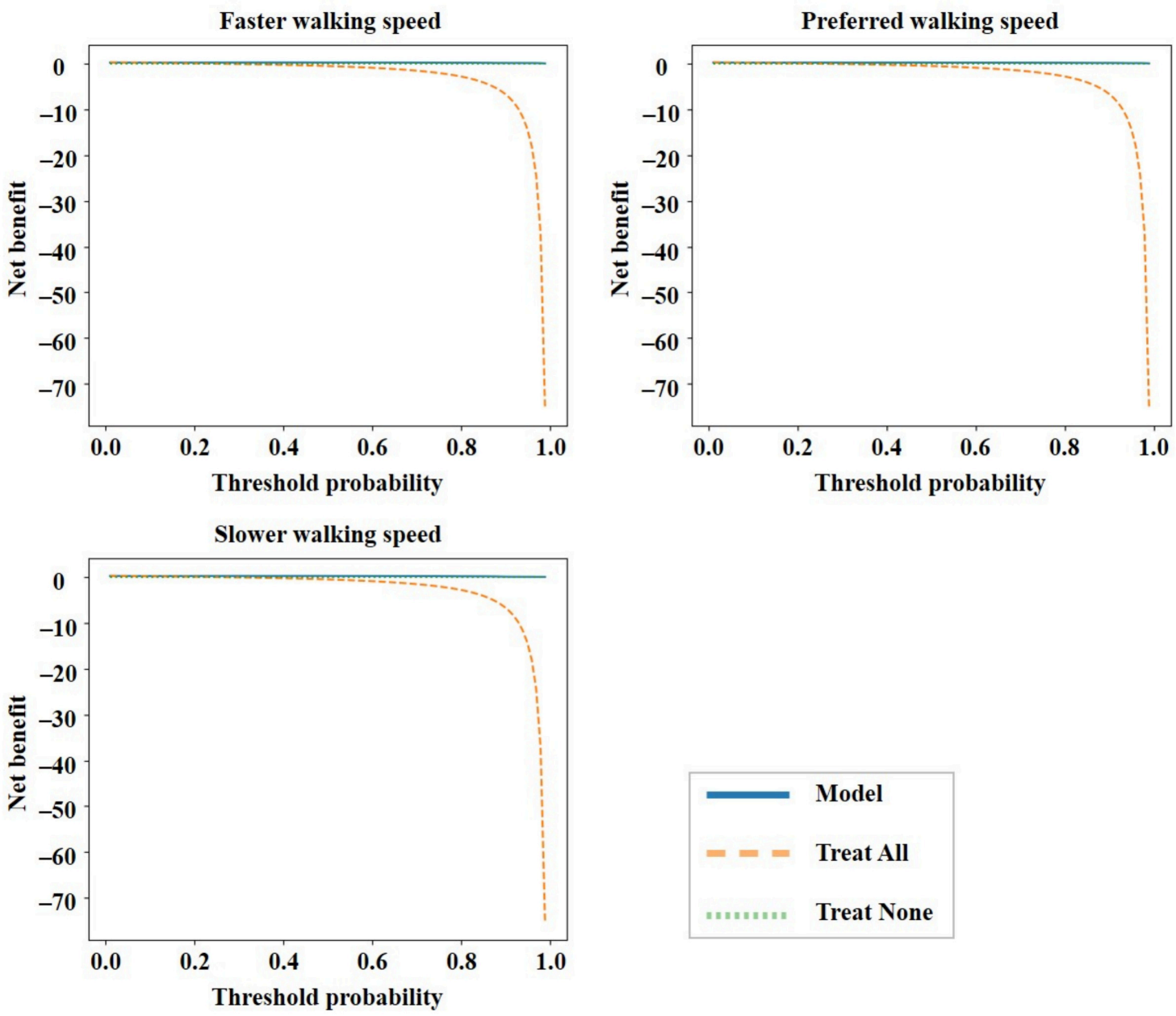


Figure 5

Decision curve analysis of subject-level Parkinson's disease (PD) transition detection using the multi-channel model. Decision curves illustrate the net benefit of using the subject-level mean PD-likeness score to identify transition cases under faster, preferred, and slower walking conditions. The solid line represents the proposed multi-channel model, while the dashed and dotted lines represent the treat-all and treat-none strategies, respectively. The x-axis indicates the threshold probability used to define a positive decision, and the y-axis represents the corresponding net benefit. Across a wide range of threshold probabilities, the model provided higher net benefit than both alternative strategies, indicating potential clinical utility for subject-level transition detection.

Supplementary Files

This is a list of supplementary files associated with this preprint. Click to download.

- Supplementaryfile1.SupplementaryTableS1.docx